NASA TECHNICAL MEMORANDUM

NASA TM X-73434

NASA TM X-73434

(NASA-TM-X-73434) PRELIMINARY SCALING LAWS FOR PLASMA CURRENT, ION KINETIC TEMPERATURE, AND PLASMA NUMBER DENSITY IN THE NASA LEWIS BUMPY TORUS PLASMA (NASA) 29 p HC $4.00 CSCL 201 G3/75

N76-28014

Unclas 42400

PRELIMINARY SCALING LAWS FOR PLASMA CURRENT, ION KINETIC TEMPERATURE, AND PLASMA NUMBER DENSITY IN THE NASA LEWIS BUMPY TORUS PLASMA

by J. Reece Roth
Lewis Research Center
Cleveland, Ohio 44135

TECHNICAL PAPER presented at the Third International Conference on Plasma Science sponsored by the Institute of Electrical and Electronics Engineers
Austin, Texas, May 24-26, 1976

PRELIMINARY SCALING LAWS FOR PLASMA CURRENT, ION KINETIC TEMPERATURE, AND PLASMA NUMBER DENSITY IN THE NASA LEWIS BUMPY TORUS PLASMA

by J. Reece Roth

Lewis Research Center

E-8783

ABSTRACT

Parametric variation of independent variables which may affect the characteristics of the NASA Lewis Bumpy Torus plasma have identified those which have a significant effect on the plasma current, ion kinetic temperature, and plasma number density, and those which do not. Empirical power-law correlations of the plasma current, and the ion kinetic temperature and number density were obtained as functions of the potential applied to the midplane electrode rings, the background neutral gas pressure, and the magnetic field strength. Additional parameters studied include the type of gas, the polarity of the midplane electrode rings (and hence the direction of the radial electric field), the mode of plasma operation, and the method of measuring the plasma number density. No significant departures from the scaling laws appear to occur at the highest ion kinetic temperatures or number densities obtained to date.

INTRODUCTION

The characteristics and performance of the superconducting NASA Lewis Bumpy Torus Magnet Facility have been described elsewhere (refs. 1 and 2). The properties and behavior of the plasma created in this facility have been discussed in a series of reports (refs. 3 to 12). The NASA Lewis Bumpy Torus experiment is characterized by three factors:

(1) The plasma, magnetic field, and ion heating mechanism are operated in the steady state.

(2) The ion kinetic temperature is typically more than a factor of 10 higher than the electron temperature.

(3) The plasma is acted on by a combination of strong dc magnetic and electric fields.

The presence of strong radial electric fields acting on the plasma, which usually exceed values of 1 kilovolt per centimeter, not only is responsible for heating the ions to kinetic temperatures on the order of kilovolts, but also affect

the dynamics and radial transport of the plasma. Previous investigations (refs. 13 to 16) have shown that, in common with Penning discharges and magnetron-like devices, the plasma forms rotating spokes which gyrate around the minor circumference of the plasma with velocities comparable to the E/B drift velocity; and the ions in these rotating spokes then form an energy reservoir which is thermalized to the high kinetic temperatures observed. The strong radial electric fields also have a profound effect on the radial transport of plasma.

Previous investigations (refs. 3 and 10) have shown that the average particle residence time of the ions is virtually independent of the magnetic field over a factor of 10 variation in the magnetic field strength. This previous work indicated that the ion heating and radial transport processes in the NASA Lewis Bumpy Torus differ substantially from those in stellarators, tokamaks, and other conventional approaches which rely on pure magnetic containment of the plasma. It was therefore deemed of interest to investigate the parametric scaling laws for the plasma current and the ion kinetic temperature and number density in the Bumpy Torus plasma to see whether scaling laws could be obtained over a range of an order of magnitude or more in the independent variables which have been investigated thus far. Such empirically derived scaling laws might afford a clue to the physical processes responsible for the radial transport of plasma in this device, and also might confirm the ion heating mechanism which has been investigated both theoretically and experimentally on a prototype mirror machine facility (refs. 14 and 15). The data on which the correlations of this report are based were taken over a period of $2\frac{1}{2}$ years, and amounted to nearly 800 individual experimental runs.

The approximate ranges over which the independent and dependent variables ranged in this series of experiments are listed in table I. The dc power input to the plasma ranged over at least six orders of magnitude, from less than 1/10 of a watt to more than 150 kilowatts. At present, arcing within the vacuum tank and flashover of the external insulators limits the potential which can be applied to the electrode rings, and the total current and power drawn by the plasma are limited by uncooled sheet metal and glass viewports in the vacuum tank.

CORRELATION PROCEDURE

The dependent variables chosen to be correlated include the ion number density and kinetic temperature; and the plasma current flowing to the electrode rings, which is a dependent variable characteristic of the modified Penning discharge ion heating scheme used in the NASA Lewis Bumpy Torus. The plasma current is also a measure of the total particle loss rate from the confined plasma.

In the absence of an adequate understanding of the physical processes in the plasma, it was assumed that these three dependent variables could be correlated by power law relations of the form

$$I_p = C_1 V_A^{\alpha_{11}} p_o^{\alpha_{31}} B_{max}^{\alpha_{41}} n_e^{\alpha_{51}} \tag{1}$$

$$T_i = C_2 V_A^{\alpha_{12}} I_p^{\alpha_{22}} p_o^{\alpha_{32}} B_{max}^{\alpha_{42}} n_e^{\alpha_{52}} \tag{2}$$

$$n_e = C_3 V_A^{\alpha_{13}} I_p^{\alpha_{23}} \rho_o^{\alpha_{33}} B_{max}^{\alpha_{43}} \tag{3}$$

Each dependent variable was assumed to be a power law function of the three variables which can be independently varied in the laboratory, the anode voltage in kilovolts, the background neutral gas pressure in the vacuum tank measured in microtorr, and the maximum magnetic field on the magnetic axis of the plasma in tesla. Also included were the electron number density in particles per cubic centimeter and plasma current in amperes, which were considered possible independent variables of a physical theory describing the dependent variables. Exceptions were equations (1) and (3), where the dependent variable was not included on the right-hand side of the equation, that is, α_{21} is identically equal to zero in equation (1), and α_{53} was identically equal to zero in equation (3).

Having chosen the power laws in equations (1) to (3), the possibility must be recognized that one or more of the parameters included on the right-hand side of these equations may not be an appropriate correlation parameter. A parameter may not be appropriate for at least two reasons: The parameter may be irrelevant to the physical processes which determine the quantity on the left-hand side of the equation; or the parameter may be inappropriate because two or more of the variables on the right-hand side of the equation may be implicit functions of one another, or related to each other by physical processes which do not allow them to be treated as though they were independent variables. In the second case, such implicit dependences among the variables violate the fundamental assumption that the variables being correlated are statistically independent.

To allow for the possibility that one or more of the variables might be irrelevant in equations (1) to (3), one or more of the exponents on the right-hand side of these equations were set equal to zero according to the scheme described in table II. In set no. 1, all of the variables in equations (1) to (3) were permitted to vary. In sets no. 2 to 9, one or more of the "independent" variables was omitted from the correlation.

The power law expressions in equations (1) to (3) were converted to simple linear polynomials by taking the logarithms of both sides and treating the exponents α_{ij} as unknowns which were to be determined by obtaining the best fit consistent with the experimental data for the variables which they multiply. The best-fitting power law exponents α_{ij} were obtained by a statistical procedure which is described in reference 17. This procedure not only provided the best-fitting values of α_{ij} consistent with the experimental data of table III, but it also provided two quantities which are useful in specifying quantitatively how good is the fit to the experimental data. The first of these quantities is the RMS normalized residual, which is given by the square root of equation 4.22 in reference 17. For brevity, this RMS normalized residual will be called the "error," and gives a measure of how far the experimental data points lie from the best-fitting pow - law given in equations (1) to (3). The larger the error, the further away are the experimental points from the value predicted by the power law relationship.

An example of the physical significance of the "error" may be seen in figure 1, in which the measured value of the plasma current is plotted on the x-axis and the right-hand side of equation (1) for the best-fitting values of α_{ij} is plotted on the y-axis for run series UY-VJ. If the correlation law were exact, all of the data would lie along the straight line with slope of 45° and the error would be zero. In this instance, the data for the low pressure mode, designated by the letter "A", has an error of 0.221; and these data points lie very close to the line of agreement. However, the high pressure mode data, designated by the letter "B", has an error of 1.01, five times as high; and the spread of the data from the line of agreement is much greater. Naturally, one would like this error to be as small as possible. The smallness of the "error" was used as the primary criterion for choosing among the nine sets of correlations listed in table II.

The correlation procedure also produced a second quantity which is equal to the square root of the left-hand side of equation 4.23 in reference 17, which we will call the "pseudo-variance." This pseudo-variance may be thought of as the error bars on the parameters α_{ij}. The pseudo-variance becomes smaller as the fit to the experimental data becomes better, and it becomes smaller as the population of data points which is used to determine the exponents α_{ij} becomes larger. Large values of the pseudo-variance imply a small number of data points and/or a poor fit to the experimental data.

EXPERIMENTAL DATA POPULATION

The experimental data, which was correlated according to the scheme described above, is listed in table III. These data were taken over a period of

$2\frac{1}{2}$ years. The first three run series used spectroscopic techniques to measure the electron temperature. The relative electron number density was obtained from the electron temperature by a procedure which is described in references 3 and 5. Unfortunately, only relative and not absolute number densities could be measured by this technique. Run series YM-YQ, ZL-ZM, and ZN1-ZN5 used the RF emission diagnostic described by Gerdin in references 4 and 12 to measure the absolute plasma number density.

The data shown on table III represents both helium and deuterium gas, and both positive and negative polarities of the midplane electrode rings. There is one run series, YC-YJ, in which a single electrode ring was used instead of the 12 used in all other run series. Unfortunately, the electron number density was not measured for this run series. As a result, it was not useful in deriving correlations for comparison with the case of 12 electrode rings. Such comparisons will be the subject of future research.

DETERMINATION OF BEST FITTING SCALING LAWS

The experimental data listed in table III were analyzed by a computer program which performed the statistical procedure described in reference 17 for one run series at a time. For each run series, separate correlations were obtained for the high and low pressure modes of operation. The run series listed in table III were not combined into one large data population for two reasons. The first was that the computer memory capacity was inadequate to handle all of the data listed on table III. Even if this limitation could have been overcome, it was anticipated that the exponents of the scaling law or the coefficients C_j multiplying the right-hand side of equations (1) to (3), might vary with the mode of operation, the gas used, the polarity of the midplane electrode rings, or the number of electrode rings used.

The first order of business in correlating the experimental data was to determine which of the nine combinations of parameters listed in table II best correlated the available experimental data. All of the run series on table III were analyzed by the computer program, and correlations were obtained for equations (1) to (3) and for all nine sets of variables. The best-fitting correlation among the nine sets on table II had the following characteristics.

(1) The error was minimized for the best-fitting combination of parameters.

(2) The pseudo-variance of the exponents α_{ij} was minimized for the best-fitting set of variables.

(3) Five of the run series listed in table III were taken under identical conditions. The values of the best-fitting exponents should be the same for these data. For sets of parameters that were not the best-fitting ones, the values of α_{ij}

could and did differ substantially among these otherwise identical run series. For the best-fitting exponents, however, these five run series yielded nearly the same values of the exponents and the multiplying constants C_j.

Inspection of this mass of information revealed that the sets of parameters with the wavy underline in table II were those which produced the best-fitting correlations to the experimental data. That is, set 7 best fit the current correlation of equation (1), set 3 best fit the ion temperature correlation in equation (2), and set 6 best fit the electron number density correlation in equation (3). The best-fitting correlation laws therefore had the functional form listed in equations (4) to (6).

$$I_p = C_1 p_o^{\alpha_{31}} B_{max}^{\alpha_{41}} n_e^{\alpha_{51}} \tag{4}$$

$$T_i = C_2 V_A^{\alpha_{12}} B_{max}^{\alpha_{42}} \tag{5}$$

$$n_e = C_3 V_A^{\alpha_{13}} p_o^{\alpha_{33}} \tag{6}$$

Some specific examples of the best-fitting correlation laws are shown in figures 1 to 3 for one of the run series on table III. In these figures, the letter "A" denotes data taken in the low pressure mode of operation, and the letter "B" data from the high pressure mode. On the ordinates are plotted the right-hand side of equations (4) to (6), with the best-fitting values of the constant C_j and of the exponents for that particular run series. The experimentally measured value of the correlated parameter is plotted on the x-axis.

The characteristic data on figure 1 show that the data are reasonably well correlated over about three orders of magnitude in the measured plasma current, and there do not seem to be any systematic departures from the correlation laws either at the low or the high end of the operating range. Figure 2 shows the best-fitting correlations of the ion kinetic temperature for the same run series. The data scarcely range over an order of magnitude. This run series is early data in which the charge-exchange neutral detector was not at its maximum sensitivity, and in which the ion kinetic temperature was limited by the anode voltage available from the power supply which was used at that time. Data from another run series, YT-YZ, are illustrated in figure 2(b) in which the ion kinetic temperature varies over an order of magnitude. The data for both modes of operation are well correlated and do not vary from the correlation law at either the low or the high end of the operating conditions. On figure 3 are shown the best-fitting correlations

of the electron number density for the same run series illustrated in figures 1 and 2. In this case the correlations range over about two orders of magnitude and represent reasonably good fits to the data, although there appears to be difficulty at the highest densities in figure 3 where the high pressure mode varies substantially from the best-fitting correlation.

Since we are interested in extrapolating the results of the current experiment, it is important to determine if there are departures from the scaling laws near the upper limit of the parameters being correlated. This was done by determining whether there were knees or asymptotes in the plotted data on figures 1 to 3, and for similar such graphs for the other run series listed in table III. In addition to looking for departures from the line of agreement, the data were further analyzed by plotting the ratio of the right-hand side of equations (1) to (3) to the experimentally measured value of that parameter, as a function of the independent variables being correlated. This procedure is illustrated for figure 3, in which the correlated number density has a suspiciously wide spread at the high end of its range, suggesting that the correlation might break down at high densities. To investigate this behavior, figure 4 shows the ratio of the correlated to the measured value of the density as a function of the three independent variables being correlated. In figure 4(a), there is no tendency, in either mode of operation, for the correlated number density to vary systematically with the neutral gas pressure, even though the data are scattered rather widely at the higher values of neutral gas pressure. In figure 4(b) this ratio is plotted as a function of plasma current, and again there is no systematic departure from a good correlation either at the low or high end of the plasma current. Figure 4(c) shows the ratio plotted as a function of anode voltage, and there may be a slight failure of the scaling law at high anode voltage. Such a departure from the scaling law, however, was not observed in the other run series which were correlated.

DETERMINATION OF SCALING LAW EXPONENTS

After determining that the combinations of parameters underlined in table II produced the best-fitting correlations for the experimental data, the next objective is to determine whether the best-fitting values of the exponents α_{ij} differ systematically with the conditions under which the data were taken, that is, whether the exponents differ with the type of gas used, the polarity of the electrode ring, or the mode of operation. The best-fitting exponents for each run series which could be correlated are shown in figures 5 to 7 along with the pseudo-variance, which provides error bars for the exponent. There did not

appear to be any systematic dependence of the exponents on the type of gas used, the polarity of the electrode rings, or the mode of operation. There did not seem to be any systematic effect on the ion kinetic temperature correlation of the single case on figure 7 in which only one electrode ring was used.

The vertical lines in figures 5 to 7 represent an effort by the author to define a compromise exponent which would apply to the entire data population. These overall best-fitting value of α_{ij} are listed in table IV for the scaling laws given in equations (4) to (6). The total number of experimental runs represented by the data on figures 5 to 7 are summarized in the third column of table IV, and the constants which multiply equations (4) to (6) are listed under table IV. While there did not appear to be any systematic dependence of the exponents on the operating conditions listed, the constants C_j which multiply the scaling relationships did depend on these external factors.

The value of the constant C_1, which determines the current drawn by the plasma, depends both on the mode of operation and on the polarity of the electrode rings.

The constant C_2, which multiplies equation (6) for the ion kinetic temperature correlation, does not depend on the polarity of the electrode rings, the mode of operation, or the gas used. This is illustrated by data from reference 4, shown in figure 8, in which the ion kinetic temperatures were measured under identical conditions of gas pressure, magnetic field, and anode voltage with both positive and negative polarities applied to the midplane electrode rings. In figures 8(a) and (b) the ion kinetic temperature and the ion heating efficiency do not depend on the electrode polarity. That the constant C_2 is apparently the same for both deuterium and helium gas is somewhat surprising, although the theoretical expression for the ion kinetic temperature derived in reference 15 predicts that the ion kinetic temperature is proportional only to the fourth root of the particle mass ratio. The 16 percent difference that results from use of helium instead of deuterium would probably not be resolvable with the current data.

The coefficient C_3 multiplying the density correlation differs only with the polarity of the midplane electrode rings, and is about a factor of 4 lower for negative polarities than with positive electrode rings. It is interesting to note on figure 7 that the exponents of the density correlation are the same for those run series in which the relative number density was measured by spectroscopic means, and for those in which the absolute number density was measured by the RF emission technique of Gerdin. This agreement of the scaling relationships for the two sets of density data reinforces Gerdin's conclusion (refs. 4 and 12) that the RF emission peak near the lower hydrid frequency enabled him to measure a quantity proportional to the plasma number density. On figure 9 are shown

some data from reference 4 in which Gerdin plotted the relative density from spectroscopic measurements on the ordinate and the absolute number density from the RF measurements on the abscissa. They tended to fall around a 45^{o} line of agreement. Gerdin's data were characteristic of an emitting region in the plasma, which may be a region of maximum density. The spectroscopic data, however, represented a time and space average across the plasma diameter.

PHYSICAL IMPLICATIONS OF SCALING LAWS

The best-fitting scaling laws may be written down by substituting the exponents from table IV in equations (4) to (6) to yield:

$$I_p = C_1 p_o^{1.10} B_{max}^{0.25} n_e^{1.0} \quad \text{amps} \tag{7}$$

$$T_i = C_2 V_A^{0.70} B_{max}^{0.30} \quad \text{eV} \tag{8}$$

$$n_e = C_3 V_A^{1.10} p_o^{0.40} \quad /\text{cm}^3 \tag{9}$$

where the constants C_1 to C_3 are given on table IV. When scaling the plasma current, it is often desirable to have only independent variables on the right-hand side. This may be obtained by substituting equation (9) into equation (7) to obtain

$$I_p = D_1 V_A^{1.10} p_o^{1.50} B_{max}^{0.25} \quad \text{amps} \tag{10}$$

where the constant D_1 is given by

$$D_1 = C_1 C_3 = \begin{cases} 3.8\times10^{-4} & A/(\mu T)^{1.5}\,(kV)^{1.1}\,(T)^{0.25} \quad \text{HPM} \quad + \\ 1.5\times10^{-4} & A/(\mu T)^{1.5}\,(kV)^{1.1}\,(T)^{0.25} \quad \text{LPM} \quad + \\ 3\times10^{-4} & A/(\mu T)^{1.5}\,(kV)^{1.1}\,(T)^{0.25} \quad \text{Both} \quad - \end{cases}$$

These scaling laws have some interesting implications. To the extent that these exponents represent a good compromise among the individual run series shown in figures 5 to 7, then this implies that the physical processes which govern the four parameters correlated in equations (7) to (9) are the same regardless of the mode of operation, the type of gas, or the polarity of the midplane

electrode rings. This similarity of the physical processes is particularly surprising for the two modes of operation. In references 3 and 4 evidence was presented which seemed to indicate that different physical processes may have been affecting the radial transport of particles in the two modes of operation. The above correlation laws appear to suggest that the physical processes occurring in the plasma are the same in the two modes, and the different currents represented by the differing values of C_1 in the two modes of operation are merely the result of a geometric or boundary condition effect, rather than representing an entirely different physical process.

The electron number density in equation (9) does not depend on the mode of operation. The value of C_3 is the same in both modes for the RF derived number density measurements, but the relative number densities obtained spectroscopically differ between one and two orders of magnitude for the two modes. The value of C_3 in table IV is taken from the RF data. The reason why a substantial modal density difference occurred in the spectroscopic data but not in the RF data must await determination by future measurements with a microwave interferometer.

The relationship between the plasma current and the other variables shown in equation (7) may be understood on the following basis: The continuity equation for charged particles in the Bumpy Torus plasma may be written in the form

$$\frac{dn_e}{dt} = n_e n_o \langle \sigma v \rangle_{ne} - \frac{I_p}{e V_p} \tag{11}$$

where the first term on the right-hand side is the volume production rate of charged particles in the plasma, and the second term is the volume rate of loss, where the plasma current I_p is the total rate of loss of particles from the plasma, and V_p is the plasma volume. In the steady state, one can set the left-hand side of equation (11) equal to zero and obtain

$$I_p = eV_p n_e n_o \langle \sigma v \rangle_{ne} \tag{12}$$

Equation (12) demonstrates that when the plasma current is due to volume ionization, it is proportional to the product of the neutral and charged particle number density. This is very close to the empirical scaling law of equation (7). It is therefore possible to understand equation (7) as a consequence of the plasma current being created by volume ionization in the plasma, and not by conditions on the boundary, collection of parasitic currents, or by emission from one or another of the electrodes used.

Equation (8) for the ion kinetic temperature is not the functional dependence which one would expect from simplistic physical arguments. It has been shown in references 3, 4, 14, 15, and 16 that the ions are heated by E×B rotation in the crossed electric and magnetic fields of the plasma. On this basis, one might expect the ion kinetic temperature to be given in terms of the E/B drift velocity as follows,

$$T_i = \frac{1}{2} m_i v_{de}^2 = \frac{1}{2} m_i \frac{E_r^2}{B^2} \approx \frac{1}{2} m_i \frac{V_A^2}{R^2 B^2} \tag{13}$$

where the average electric field is assumed to be the electrode potential divided by the plasma radius. The oversimplified model of equation (13) therefore predicts an ion kinetic temperature proportional to the ion mass, proportional to the square of the electrode potential, and inversely proportional to the square of the magnetic field.

In reference 15 a theory taking into account finite gyroradius effects, and which assumes that the ion mobility is higher than the electron mobility, yielded the theoretical expression for the ion kinetic temperature given in equation (14).

$$T_i = \frac{V_A}{\pi B^{1/2}} \left(\frac{8 m_i n_e}{\xi^2 \epsilon_o} \right)^{1/4} \quad eV \tag{14}$$

This theory predicts that the ion kinetic temperature is proportional to the fourth root of the ion mass, to the fourth root of the electron number density, inversely proportional to the square root of the magnetic field, and directly proportional to anode voltage.

The empirical scaling law in equation (8) is much closer to the theoretical expression derived for the modified Penning discharge in equation (14) than it is for the simple E×B drift model. The weak dependence on electron number density predicted by equation (14) may be beyond the resolution of the current data and does not necessarily represent a discrepancy. The differences between the exponents on the electrode potential and magnetic field are substantial, and probably represent a discrepancy larger than the uncertainty of the current data set.

DISCUSSION

Several parameters which are known to affect the plasma characteristics have not yet been optimized. These parameters include the number of electrode

rings used to generate the plasma; the alignment of the electrode rings with respect to the magnetic field drift surfaces; and the presence, direction, and magnitude of a weak vertical magnetic field imposed parallel to the major axis of the torus. Systematic variation of these three parameters has been awaiting installation and operation of a microwave interferometer system so that reliable absolute electron number density measurements could be made. If changing these three parameters degraded the plasma characteristics and made the scaling laws discussed above less favorable, one could leave them at their existing values without penalty.

There is reason to suppose that the variation of one or more of these parameters will substantially improve the electron number density obtained. On figure 10 is shown some spectroscopic data taken by R. W. Richardson which shows the relative electron number density as a function of the number of anode rings. The electron number density increases substantially as the number of anode rings is decreased. In the low pressure mode of operation, the relative electron number density increased by about a factor of 5 as the number of anode rings was reduced from 12 to 6. In the high pressure mode of operation, the relative electron number density increased by about a factor of 10 as the number of anode rings was reduced from 12 to 3. If these trends are confirmed by subsequent data taken with a microwave interferometer, it may be possible to increase the constant which multiplies the scaling law of equation (10) for the electron number density by a factor of 5 to 10 if the optimum number of electrode rings are used.

Figure 11 suggests what may be an effect on the ion kinetic temperature and ion heating efficiency of the number of anode rings used to generate the plasma. Shown on figure 11(a) is the ion kinetic temperature with 12 anode rings on the ordinate, and the ion kinetic temperature measured under the same conditions with only a single anode ring used to energize the plasma on the abscissa. There does not appear to be any significant difference in the ion kinetic temperatures in the low pressure mode of operation, but in the high pressure mode of operation 12 electrode rings appear to heat the plasma more effectively than a single one. This same general trend for the same data population is exhibited in figure 11(b) which shows the ion heating efficiency for 12 and 1 anode rings.

Thus, the available data seem to indicate that it may be possible to improve on the results implied by the scaling laws derived above, if the remaining experimental parameters are optimized.

SUMMARY

Parametric variation of independent variables which may affect the characteristics of the NASA Lewis Bumpy Torus have identified those which have a significant effect on the plasma current, ion kinetic temperature and number density, and those which do not. Empirical scaling laws which relate these parameters to the midplane electrode voltage, magnetic field, and neutral gas pressure were obtained from a series of experimental runs containing several hundred data points and an order of magnitude or more variation in the latter variables. The best-fitting scaling laws were found to be as follows.

$$I_p = D_1 V_A^{1.10} p_o^{1.50} B_{max}^{0.25} \quad \text{amps}$$

$$T_i = C_2 V_A^{0.70} B_{max}^{0.30} \quad \text{eV}$$

$$n_e = C_3 V_A^{1.10} p_o^{0.40} \quad /\text{cm}^3$$

In addition to the continuous independent variables correlated above, additional parameters which affect the plasma properties were also varied including the polarity of the midplane electrode rings (which determines the direction of the radial electric field), the number of midplane electrode rings, the mode of plasma operation, and the method of measuring the plasma number density.

The scaling laws derived from the data remained valid over an order of magnitude or more in the dependent parameters being correlated and showed no tendency to break down at the highest plasma currents and ion energies and densities which were attainable in the current series of experiments. The conditions at the upper limits were sufficient to exhibit small but measurable steady-state neutron production from DD reactions in a deuterium plasma.

REFERENCES

1. J. R. Roth, et al., "Characteristics and Performance of a 12-Coil Superconducting "Bumpy Torus" Magnet Facility for Plasma Research," NASA TN D-7353, Aug. 1973.

2. J. R. Roth, et al., "A 12-Coil Superconducting "Bumpy Torus" Magnet Facility for Plasma Research," in Fifth Applied Superconductivity Conference, Institute of Electrical and Electronics Engineers, 1972, pp. 361-366.

3. J. R. Roth, G. A. Gerdin, and R. W. Richardson, "Characteristics of the NASA Lewis Bumpy Torus Plasma Generated with Positive Applied Potentials," NASA TN D-8114, March 1976.

4. J. R. Roth and G. A. Gerdin, "Characteristics of the NASA Lewis Bumpy Torus Plasma Generated with High Positive or Negative Applied Potentials," NASA TN D-8211, April 1976.

5. R. W. Richardson, "Spectroscopic Results in Helium Gas from the NASA Lewis Bumpy Torus Plasma," NASA TM X-71569, May 1974.

6. G. A. Gerdin, "Spoke Wavenumbers and Mode Transitions in the NASA Lewis Bumpy Torus," NASA TM X-71624, 1974.

7. J. R. Roth, R. W. Richardson, and G. A. Gerdin, "Initial Results from the NASA Lewis Bumpy Torus Experiment," NASA TM X-71418, Nov. 1973.

8. R. W. Richardson, "Effect of Anode Ring Arrangement on the Spectroscopic Characteristics of the NASA Lewis Bumpy Torus Plasma," NASA TM X-71636, Oct. 1974.

9. G. A. Gerdin, "Radio Frequency Studies in the NASA Lewis Bumpy Torus," NASA TM X-71567, May 1974.

10. J. R. Roth, "Ion Heating and Containment in the NASA Lewis Bumpy Torus Plasma," NASA TM X-71630, Oct. 1974.

11. H. Persson, "Time-Dependent Outgassing and Impurities in the NASA Lewis Bumpy Torus," NASA TM X-71639, Oct. 1974.

12. G. A. Gerdin, "The Lower Hybrid Oscillation as a Diagnostic Tool," to be published.

13. J. R. Roth, "Experimental Study of Spectral Index, Mode Coupling, and Energy Cascading in a Turbulent, Hot-Ion Plasma," Phys. Fluids, vol. 14, pp. 2193-2202, Oct. 1971.

14. J. R. Roth, "Origin of Hot Ions Observed in a Modified Penning Discharge," Phys. Fluids, vol. 16, pp. 231-236, Feb. 1973.

15. J. R. Roth, "Hot Ion Production in a Modified Penning Discharge," IEEE Trans. on Plasma Sci., vol. 1, pp. 34-45, Jan. 1973.

16. J. R. Roth, "Energy Distribution Functions of Kilovolt Ions in a Modified Penning Discharge," Plasma Physics, vol. 15, pp. 995-1005, Oct. 1973.

17. P. Cziffra and M. J. Moravcsik, "A Practical Guide to the Method of Least Squares," California University, Lawrence Radiation Lab., Berkeley, Calif., Rept. UCRL-8523 (Rev.), June 1959.

TABLE I. - RANGE OF EXPERIMENTAL PARAMETERS[a]

Parameter	Helium		Deuterium	
	Lowest value	Highest value	Lowest value	Highest value
Anode voltage V_a, kV	1	50	1	50
Plasma current I_p, A	0.001	5.5	0.001	7.0
Input power W_p, watts	0.15	10^5	0.03	1.5×10^5
Maximum magnetic field B_{max}, T	0.24	2.7	0.24	3.0
Background pressure P_o, torr	5.5×10^{-6}	1.9×10^{-4}	3.7×10^{-6}	1.32×10^{-4}
Electron temperature T_e, eV	11	95	14	140
Ion temperature T_i, eV	650	3300	160	2500
Number density on axis, $n_e(0)/cm^3$	$\sim10^8$	10^{11}	$\sim10^8$	1.1×10^{11}

[a]These represent extreme and not simutaneously measured values.

TABLE II. - COMBINATIONS OF VARIABLES CORRELATED

Set number	I_p, function 1					T_i, function 2					n_e, function 3				
	α_{11}	α_{21}	α_{31}	α_{41}	α_{51}	α_{12}	α_{22}	α_{32}	α_{42}	α_{52}	α_{13}	α_{23}	α_{33}	α_{43}	α_{53}
1	V	–	V	V	V	V	V	V	V	V	V	V	V	V	–
2	V	–	V	V	0	V	V	0	V	V	V	0	V	V	–
3	V	–	V	0	0	V	0	0	V	V	V	V	0	V	–
4	V	–	V	0	V	V	0	V	V	V	V	0	0	V	–
5	V	–	0	V	V	V	0	V	V	0	V	V	V	0	–
6	V	–	0	0	V	V	V	V	V	0	V	0	V	0	–
7	0	–	V	V	V	V	0	V	0	V	0	V	V	V	–
8	0	–	V	V	V	V	V	0	0	V	0	V	0	V	–
9	0	–	V	0	V	V	0	0	0	V	0	0	V	V	–

V variable to be correlated

0 exponent set equal to zero

– variable not in correlation

TABLE III. - PARAMETERS VARIED DURING EACH EXPERIMENTAL RUN SERIES

Run series	Gas used	Number of electrode rings	Polarity of electrode rings	I_p, function 1					T_i, function 2					n_e, function 3				
				α_{11}	α_{21}	α_{31}	α_{41}	α_{51}	α_{12}	α_{22}	α_{32}	α_{42}	α_{52}	α_{13}	α_{23}	α_{33}	α_{43}	α_{53}
SN-TJ	D_2	12	+	V	–	V	V	V	V	V	V	V	V	V	V	V	V	–
UY-UJ	He	12	+	V	–	V	0	V	V	V	V	0	V	V	V	V	0	–
UI-WC	D_2	12	+	V	–	V	0	V	V	V	V	0	V	V	V	V	0	–
YC-YJ	D_2	1	+	V	–	V	0	0	V	V	V	0	0	0	0	0	0	–
YM-Y9	D_2	12	+	V	–	V	V	V	0	0	0	0	0	V	V	V	V	–
YT-YZ	D_2	12	+	V	–	V	V	0	V	V	V	V	0	0	0	0	0	–
ZA-ZI	D_2	12	–	V	–	V	V	0	V	V	V	V	0	0	0	0	0	–
ZD-ZE	He	12	+	V	–	V	0	0	V	V	V	0	0	0	0	0	0	–
ZL-ZM	D_2	12	+	V	–	V	V	V	0	0	0	0	0	V	V	V	V	–
ZN1-ZN5	D_2	12	–	V	–	V	V	V	0	0	0	0	0	V	V	V	V	–

V variable during experimental run
0 constant during run
– variable not in correlation

TABLE IV. - PRELIMINARY SCALING LAWS FOR BUMPY TORUS

Variable correlated	Best fitting set number	Total experimental runs	Constant	Parameter exponents				
				α_1, V_A	α_2, I_p	α_3, p_o	α_T, B_{max}	α_5, n_e
I_p	7	792	C_1	0	--	1.10	0.25	1.0
T_i	3	603	C_2	.70	0	0	.30	0
n_e	6	793	C_3	1.10	0	.40	0	---

		Mode	Polarity
C_1 =	1.73×10^{-13} A/$(\mu T)^{1.1}$ $(T)^{0.25}$ $(ELE/cm^3)^{1.0}$	HPM	+
	6.82×10^{-14}	LPM	+
	5.45×10^{-13}	Both	-
C_2 =	160 eV/$(kV)^{0.70}$ $(T)^{0.3}$		
C_3 =	2.2×10^{9}		+
	5.5×10^{8} $cm^{-3}/(kV)^{1.1}$ $(\mu T)^{0.40}$		-

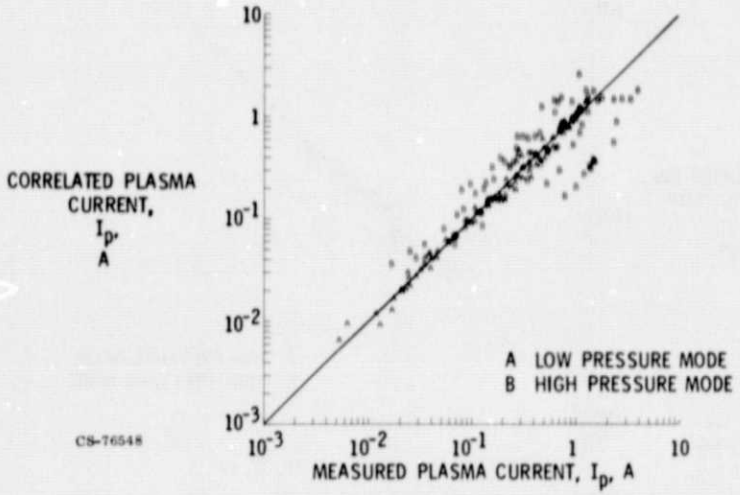

Figure 1. - The best-fitting correlation of Eq. (4) for the plasma current, as a function of the measured plasma current for run series UY-VJ. Letter "A" is the low pressure mode of operation, and "B" is the high pressure mode of operation.

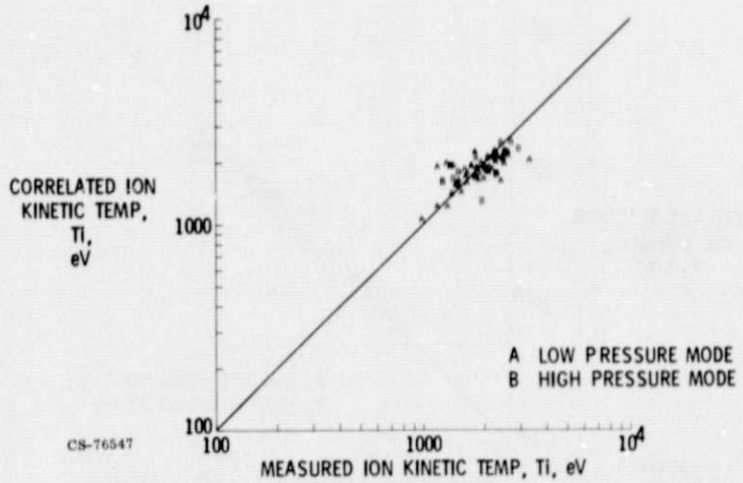

(a) RUN SERIES UY-VJ.

Figure 2. - Best-fitting correlation of ion kinetic temperature from Eq. (5) as a function of the measured ion kinetic temperature. The letter "A" is the low pressure mode of operation and "B" designates the high pressure mode of operation.

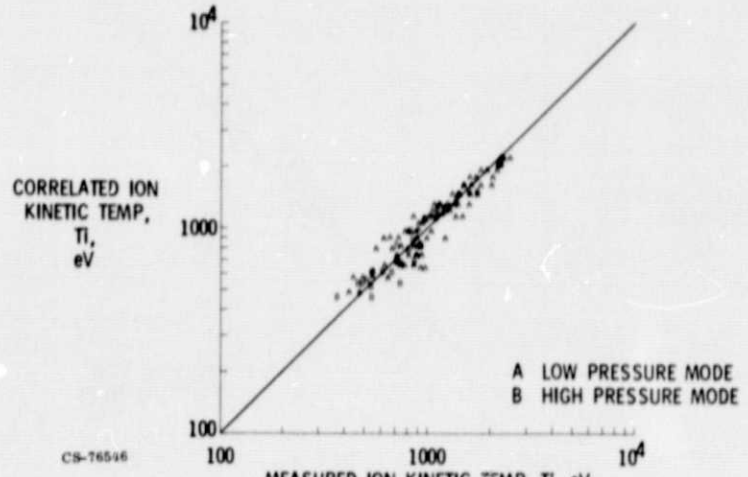

(b) RUN SERIES YT-YZ.

Figure 2. - Concluded.

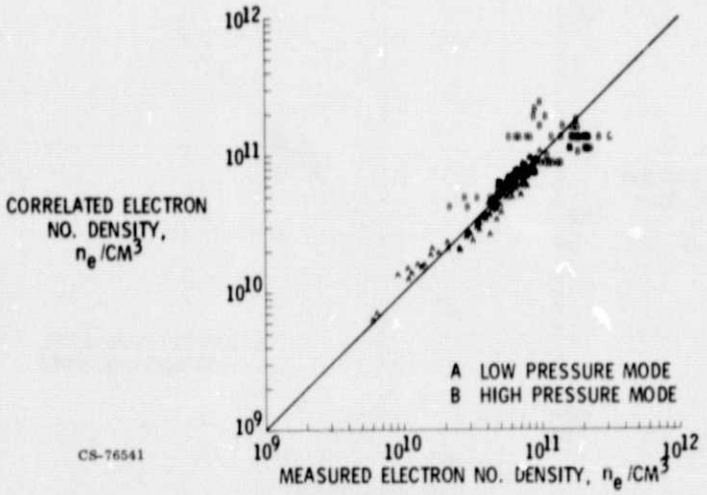

Figure 3. - The best-fitting correlation of Eq. (6) as a function of measured absolute electron number density, for run series UY-VJ. The letter "A" designates the low pressure mode of operation, and "B" the high pressure mode.

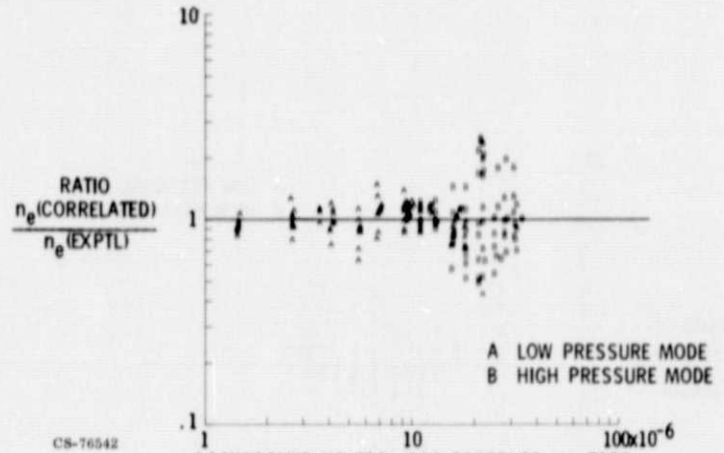

(a) THE NUMBER DENSITY RATIO AS A FUNCTION OF NEUTRAL BACKGROUND GAS PRESSURE.

Figure 4. - Ratio of the best-fitting correlation of Eq. (6) for the electron number density in run series UY-VJ, divided by the measured value of electron number density as a function of the parameters varied during this run series. The letter "A" designates the low pressure mode of operation, and "B" the high pressure mode of operation.

F-8783

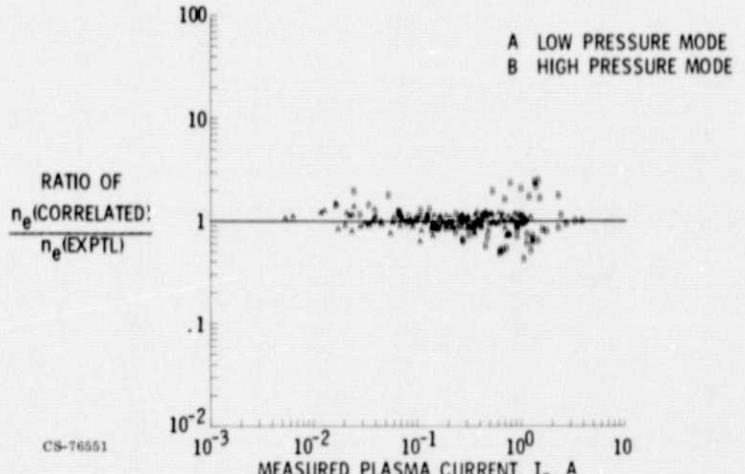

(b) THE NUMBER DENSITY RATIO AS A FUNCTION OF THE PLASMA CURRENT I_p.

Figure 4. - Continued.

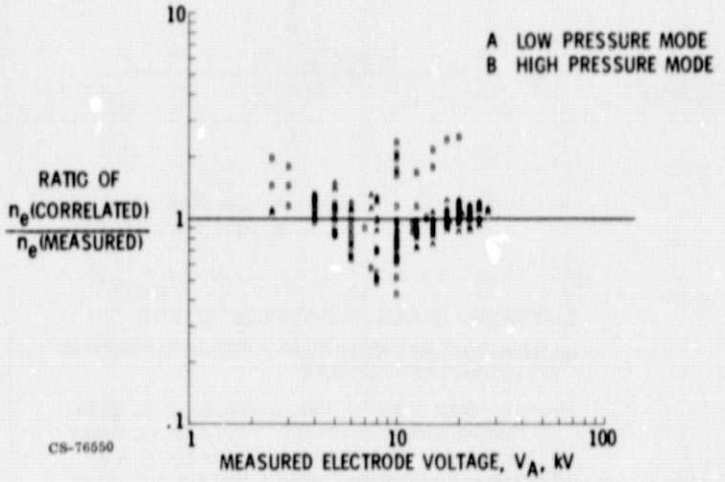

(c) THE NUMBER DENSITY RATIO AS A FUNCTION OF THE ANODE VOLTAGE.

Figure 4. - Concluded.

RUN SERIES	ERROR	NO. OF DATA POINTS	GAS	NO. OF ELECTRODES	POLARITY	MODE OF OPERATION
SN-TJ	0.833 .594	156 125	D_2	12	+	LOW HIGH
UI-WC	.306 -----	55 ---	D_2	12	+	LOW HIGH
YM-YQ	1.44	57	D_2	12	+	LOW HIGH
ZL-ZM	1.20 2.42	81 31	D_2	12	+	LOW HIGH
UY-VJ	.221 1.01	105 64	He	12	+	LOW HIGH
ZN1-ZN5	1.32 1.57	75 43	D_2	12	-	LOW HIGH

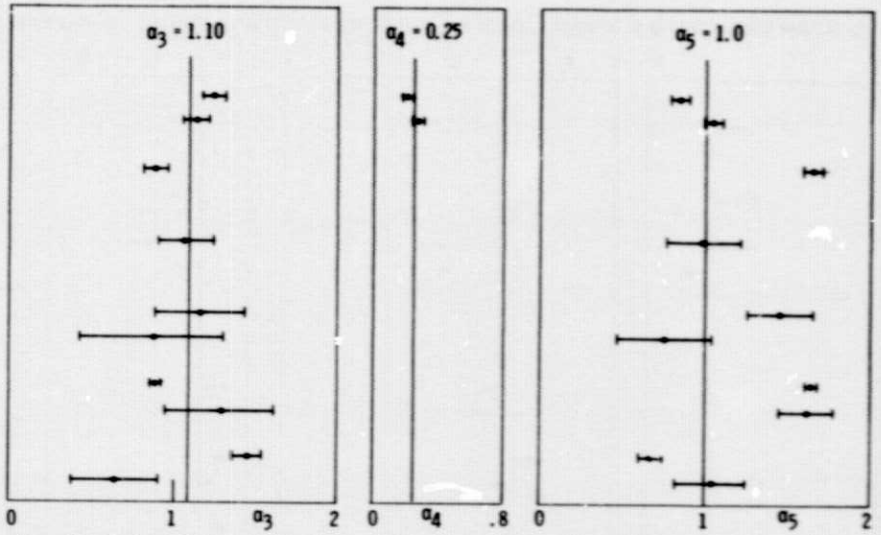

CS-76540

Figure 5. - The best-fitting exponents of the plasma current correlation of Eq. (4) for six series of runs. The author's estimate of the best-fitting average value of the exponents is indicated by the solid vertical lines.

RUN SERIES	ERROR	NO. OF DATA POINTS	GAS	NO. OF ELECTRODES	POLARITY	MODE OF OPERATION
YC-YJ	1.65 1.32	39 44	D_2	1	+	LOW HIGH
YT-YZ	.690 .591	81 26	D_2	12	+	LOW HIGH
ZA-Zi	.463 .467	48 20	D_2	12	-	[illegible] HIGH
ZD-ZE	.280 -----	18 --	He	12	+	LOW HIGH
SN-TJ	.954 1.25	130 82	D_2	12	+	LOW HIGH
UY-VJ	.765 .731	56 9	He	12	+	LOW HIGH
UI-WC	.729 -----	50 ---	D_2	12	+	LOW HIGH

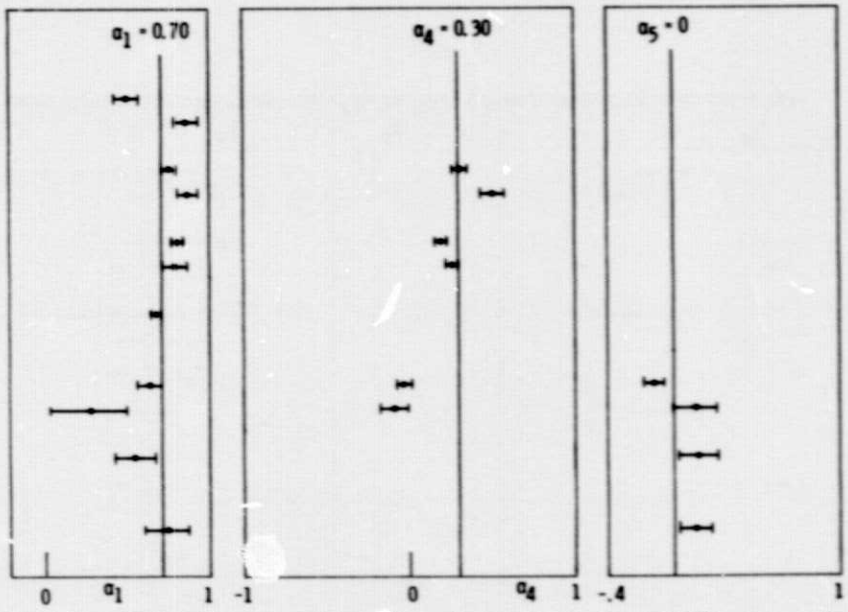

CS-76539

Figure 6. - The best-fitting exponents of Eq. (5) for the ion kinetic temperature correlation for seven series of experimental runs. The author's estimate of the best-fitting average value of the exponent is indicated by the vertical lines.

RUN SERIES	ERROR	NO. OF DATA POINTS	GAS	NO. OF ELECTRODES	POLARITY	MODE OF OPERATION
SN-TJ	1.06 .719	156 125	D_2	12	+	LOW HIGH
UI-WC	.341 -----	55 ---	D_2	12	+	LOW HIGH
YM-YQ	.984	58	D_2	12	+	LOW HIGH
ZL-ZM	.733 1.52	81 31	D_2	12	+	LOW HIGH
UY-VJ	.331 .954	105 64	He	12	+	LOW HIGH
ZN1-ZN5	.891 .773	75 43	D_2	12	-	LOW HIGH

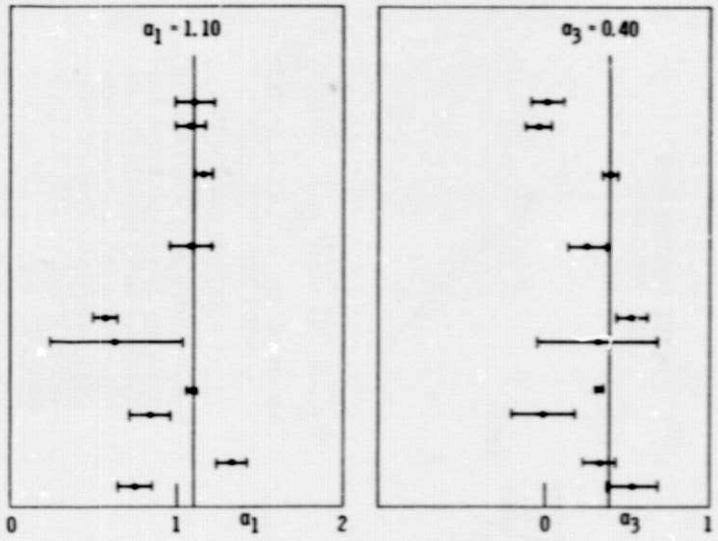

CS-76537

Figure 7. - The best-fitting exponents for the electron number density correlation of Eq. (6) for six series of experimental runs. The author's estimate of tne best-fitting average value of the exponent is indicated by the vertical lines.

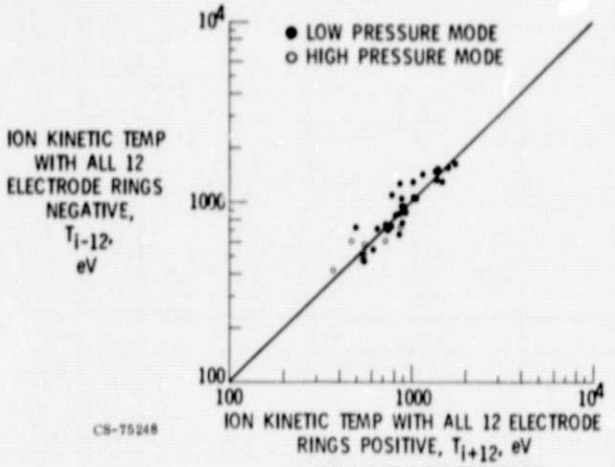

(a) ION KINETIC TEMPERATURE.

Figure 8. - Data from ref. 4 indicating that the ion kinetic temperature and ion heating efficiency do not depend on electrode ring polarity or mode of operation. Data were taken for the same magnetic fields, electrode voltages, and background neutral gas pressures.

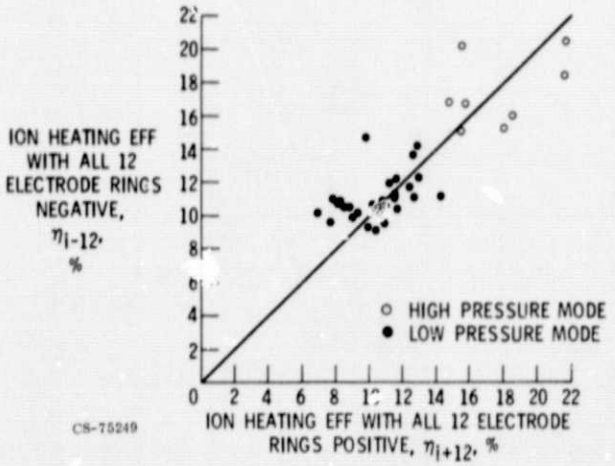

(b) ION HEATING EFFICIENCY.

Figure 8. - Concluded.

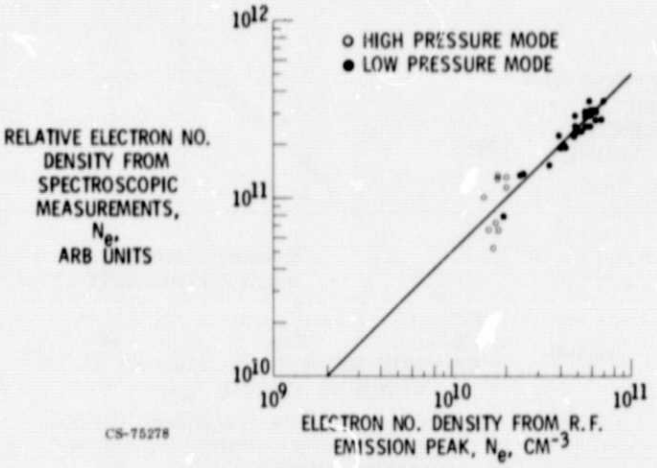

Figure 9. - Relationship between the relative number density measured spectroscopically, on the y-axis, and the absolute electron number density, measured by RF emission methods, on the x-axis. The straight line with slope of 45 degrees indicate that both diagnostic methods were measuring a quantity proportional to electron number density.

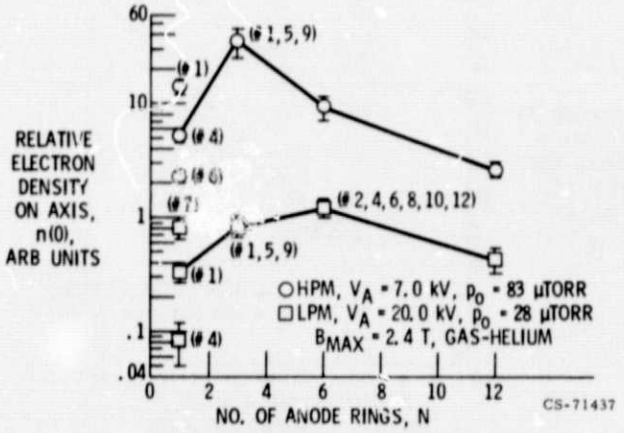

Figure 10. - Experimental data taken from ref. 3 showing the relative electron number density obtained spectroscopically as a function of the number of anode rings for the high and low pressure mode of operation, B_{max} = 2.4 tesla, and helium gas.

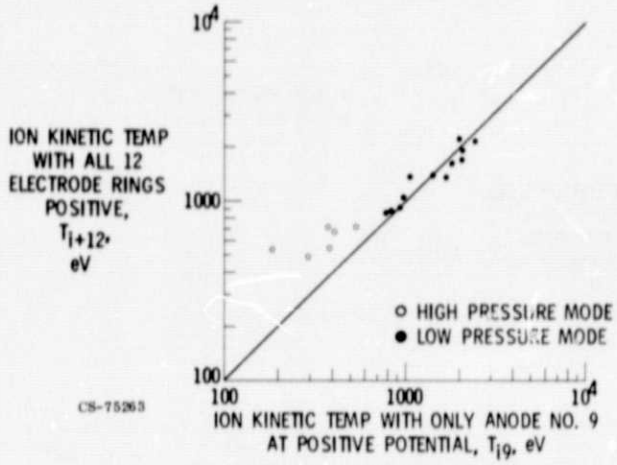

(a) ION KINETIC TEMPERATURE WITH ALL 12 ELECTRODE RINGS POSITIVE PLOTTED AGAINST THE ION KINETIC TEMPERATURE WITH ONLY ONE ELECTRODE RING ENERGIZED AND FOR THE SAME CONDITIONS OF MAGNETIC FIELD, BACKGROUND PRESSURE, AND ANODE VOLTAGE.

Figure 11. - The effect of the number of anode rings on ion kinetic temperature and ion heating efficiency, taken from ref. 4.

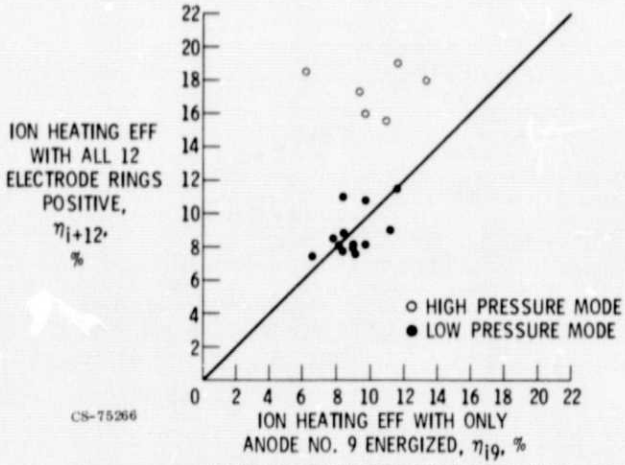

(b) THE ION HEATING EFFICIENCY WITH ALL 12 ELECTRODE RINGS POSITIVE COMPARED WITH THE ION HEATING EFFICIENCY WITH ONLY ONE ANODE RING ENERGIZED FOR THE SAME CONDITIONS OF BACKGROUND PRESSURE, MAGNETIC FIELD, AND ANODE VOLTAGE.

Figure 11. - Concluded.